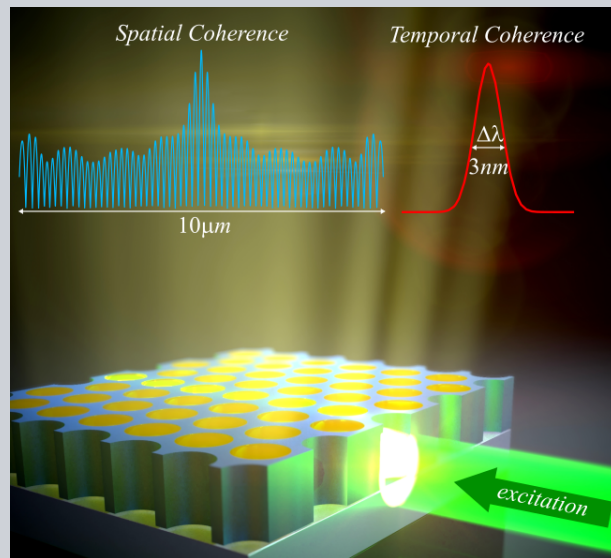


**Abstract** A class of hybrid photonic-plasmonic structures (HPPS) with vertical cylindrical cavities is proposed and its performance in providing a coherent light from spontaneous emission is investigated. It is shown that the proposed easy-to-fabricate and robust anodic aluminum oxide structure dramatically enhances the temporal and spatial coherence compared to the previously examined HPPS. The physical mechanism of achieving the temporal and spatial coherence is explained based on the special optical properties of the proposed HPPS and it is discussed how this structure enables one adjusting hybrid photonic-plasmonic optical modes to obtain coherence for emitters of different frequencies. The thorough study of the phenomenon is merely possible using a numerical method that can capture the statistical nature of a large number of fluorophores. This is in contrast to the deterministic approach that was conventionally adopted for time-domain methods. Therefore, in this paper, a numerical method is proposed, in which an innovative semi-classical probabilistic algorithm is implemented within the framework of a time-domain method.



# Fluorescence coherence with anodic aluminum oxide hybrid photonic-plasmonic structure: numerical analysis using an innovative statistical approach

Ali Reza Hashemi and Mahmood Hosseini-Farzad\*

## 1. Introduction

Fluorescence is a vastly used optical method for chemical and biological detection [1, 2]; however, its performance and efficiency shall be enhanced especially in sensing and imaging applications [3–6]. Plasmonics appears to be the best method for tailoring and enhancing the fluorescence emission [7]. It is known that light can be confined in close vicinity of metallic surfaces or nano-particles due to the coupling between electromagnetic (EM) waves and oscillations of electrical charges at the surface. The idea is to employ This interaction, which is referred to as surface plasmon resonance (SPR) in a way that a large enhancement in the optical density of states can be obtained in the neighborhood of fluorophores. This will be an effective means for elevating the excitation rate and raising the quantum yield as well as controlling the angular distribution of the fluorescence emission [8–12].

Although the presence of fluorophore in the vicinity of metallic structures leads to the above mentioned appealing features, this adjacency may also increase the probability of quenching and non-radiative energy loss for the excited fluorophore [13–16]. This inadequacy can be resolved by means of a hybrid photonic-plasmonic structure (HPPS), that is

created by attaching a photonic crystal (PC) to the metal surface (plasmonic structure). In other words, coupling between the surface plasmon polaritons (SPPs), i.e. the EM waves which are confined along the metal-dielectric interface, and the guided or trapped modes of the photonic crystal leads to the striking features of increasing the propagation length of SPPs, confining light in a deep subwavelength scale, and highly guided modes and cavity resonances in the PC structure [17–20]. Moreover, by using an HPPS, the effective length of the evanescent normal component of SPPs can extend to tens of nanometers above the metal surface, therefore, the enhancement and directionality are obtained without any significant quenching [21–23].

On the other hand, due to the weak correlation between the spontaneous emissions of fluorophores, the resulted light is isotropic in space and broad in spectrum, which in turn lower the detectability. Therefore, it is potentially advantageous to utilize a technique to create a coherent light from such spontaneous emitters. It must be noted that a desirable technique shall also prevent any significant loss in the emission intensity [24–26]. In order to address these requirements, Shi and his coworkers [27, 28] have proposed using a HPPS whose optical attributions was previously investigated by the group [29]. It is shown that the interaction between

the leaky modes (that can scape from propagating along the metal-dielectric interface) of HPPS and the fluorescent molecules successfully provides both the temporal and spatial coherence for the fluorescent emission. Such a technique can play an important role in different fluorescence applications. However, further investigations are needed to obtain a more efficient structure with an inherent capability to be adjusted for different spontaneous emitters. This is the aim of the present work.

Among different options for the photonic-crystal part of an HPPS, anodic aluminum oxide (AAO) presents a special feature; the vertical cylindrical cavities in the structure facilitates one's control over the direction of the propagation of the leaky modes. This provides the directionality of the emitted light and therefore can enhance the spatial coherence. Moreover, the frequency of the leaky modes can be adjusted by adapting the geometry of the cavities. In the literature, the capability of AAO in enhancing the intensity of fluorescent emission has also been addressed [30]. Nevertheless, AAO has not yet been used in forming an HPPS. In this work, a robust and easy to fabricate HPPS using the AAO structure is proposed that substantially enhances the coherence, while brings the required flexibility to be adjusted for spontaneous emitters with different excitation/emission frequencies.

Conducting the present study requires investigating the fluorescence emission near plasmonic nano-structures, which is still an open area for researches [3]. Considering the practical limitations of the delicate experimental setups, a rather low-cost numerical method can be effectively employed to provide guidelines for experiments [31,32] while it also advances our fundamental understanding of physical phenomena [33–36]. The conventional implementation of fluorescence in numerical methods is based on representing the molecular dipole moment of fluorophores by using a damped driven harmonic oscillator differential equation [37–39]. Nonetheless, this technique is incapable of making any distinction between the excitation and emission frequency of the molecules. More importantly, using a single deterministic equation in the numerical simulations, it is impossible to attribute statistical characteristics, e.g. coherence, to an ensemble of fluorophores. In this work, a novel algorithm is proposed to resolve this issue by introducing the probabilistic nature of the molecular transitions into the numerical method. This algorithm is implemented within the framework of finite-difference time-domain (FDTD) method [40] and validated against previously reported experimental results.

In the following, the proposed algorithm is briefly described, then, the validation test-case is modeled and results are compared with literature. The rest of this paper is dedicated to the introduction and analysis of the proposed HPPS.

## 2. Numerical modelling

Energy bands of a single fluorescent molecule can be modeled as a three (energy) level system, for which absorption and both radiative and non-radiative transitions occur [41,42] (Fig. 1). These levels are identified using three

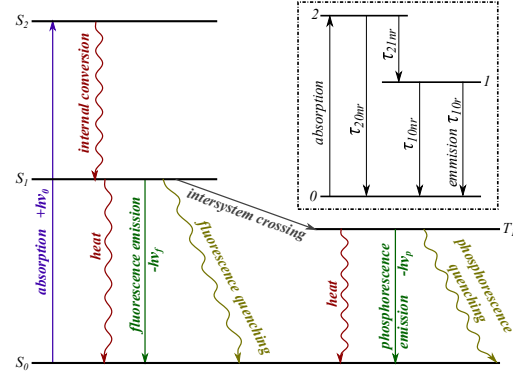


**Figure 1** Jablonski diagram showing electronic transitions of a molecule with radiative and non-radiative transitions from/to singlet ( $S$ ) and triplet ( $T$ ) states. The simplified model for a fluorescent molecule is shown in the inset.

occupation numbers  $n_0$ ,  $n_1$ , and  $n_2$ , where only one of them is 1, while the other two are 0. This is because at any instance of time, only one of the energy levels can be occupied by the molecule. The probabilities associated with possible transitions between these levels are estimated as described in the following.

**Absorption:** For the electric dipole moment of a fluorophore  $\mathbf{p}$  with maximum absorption frequency  $\omega_a$ , a forced harmonic oscillator differential equation is considered as

$$\ddot{\mathbf{p}} + \omega_a^2 \mathbf{p} = (e^2/m_e) \mathbf{E}(t), \quad (1)$$

where  $e$  and  $m_e$  are the charge and mass of electron, respectively. In this equation,  $\mathbf{E}(t)$  is the electric field imposed at the position of molecule. The resonance of  $\mathbf{p}$  leads to the absorption of energy from EM field via the Ampere-Maxwell's relation  $\epsilon \mathbf{E} = \nabla \times \mathbf{H} - \dot{\mathbf{p}}$ . The transition from level 0 to 2 becomes more probable as the energy of dipole,  $\mathbf{E} \cdot \mathbf{p}$ , gets closer to the energy difference between these levels. Therefore, the corresponding probability is estimated as

$$P_{02}(t) = \exp\left(-(\hbar\omega_a - \mathbf{E}(t) \cdot \mathbf{p}(t))^2 / \sigma_a^2\right), \quad (2)$$

where  $\sigma_a$  corresponds to the excitation bandwidth of fluorophore. It must be noted that since in the present work, the (non-)radiative decays have also been taken into the account, there is no need to explicitly introduce a damping term to Eq. (1) that in turn, improves the accuracy of the method comparing to the conventional approach.

**Non-radiative transitions:** For the present model, three non-radiative transitions are considered;  $2 \xrightarrow{nr} 1$ ,  $2 \xrightarrow{nr} 0$  and  $1 \xrightarrow{nr} 0$ . The corresponding probabilities are estimated as

$$P_{21nr}(t) = A \left(1 - \exp\left(-\frac{t}{\tau_{21nr}}\right)\right), \quad (3)$$

$$P_{20nr}(t) = B \left(1 - \exp\left(-\frac{t}{\tau_{20nr}}\right)\right), \quad (4)$$

$$P_{10nr}(t) = C \left(1 - \exp\left(-\frac{t}{\tau_{10nr}}\right)\right). \quad (5)$$

Here,  $\tau_{ijnr}$  represents the time-constant for a non-radiative decay between levels  $i$  and  $j$ . The asymptotic behavior of

these functions guaranties a definite decay at an infinitely long time.

*Radiative transition:* Radiative transition is only considered as a decay from level 1 to level 0, for which the corresponding probability is estimated as

$$P_{10r}(t) = D \left( 1 - \exp \left( -\frac{t}{\tau_{10r}} \right) \right), \quad (6)$$

where  $\tau_{10r}$  is the time constant of the radiative decay. Once the transition occurs, a wave packet with the central frequency equal to emission frequency of the fluorophore  $\omega_e$  is emitted from a point source at the position of the molecule.

The normalization factors  $A, B, C, D$  are calculated based on two physical concepts; it is impossible for a molecule to permanently stay at an excited state ( $A + B = 1$  and  $C + D = 1$ ) and the probability ratio of the transitions is inversely related to the corresponding decay times, which give

$$A = \tau_{21nr} / (\tau_{21nr} + \tau_{20nr}), \quad B = \tau_{20nr} / (\tau_{21nr} + \tau_{20nr}), \\ C = \tau_{10nr} / (\tau_{10nr} + \tau_{10r}) \quad \text{and} \quad D = \tau_{10r} / (\tau_{10nr} + \tau_{10r}).$$

In the following, the implementation of these probability functions within the framework of the developed finite-difference time-domain (FDTD) method is briefly described. It is worth noting that in this work, FDTD is utilized to simulate the propagation of EM fields in successive time-steps, while the case would be almost the same for other numerical schemes, e.g. the finite-element time-domain method.

In each time-step, the state is checked for all the molecules according to these criteria:

- For a molecule in the ground state ( $n_0 = 1$ ), it is only possible to transit into the second excited state ( $0 \xrightarrow{\text{absorb}} 2$ ) by absorbing an enough amount of energy. Computationally, this occurs if the randomly generated number  $r$  is less than (or equal to) the corresponding probability  $P_{02}(t)$  (equation 2). If the the transition does not occur, the dipole moment of the molecule is updated via the differential equation 1.
- For a molecule in the second excited state, the non-radiative decay is possible to either the first state ( $2 \xrightarrow{nr} 1$ ) or the ground state ( $2 \xrightarrow{nr} 0$ ). If random number  $r$  is less than (or equal to)  $P_{21nr}(t)$  transition  $2 \xrightarrow{nr} 1$  occurs, and on the other hand, the molecule experiences  $2 \xrightarrow{nr} 0$  if  $P_{21nr} < r \leq (P_{21nr} + P_{20nr})$ .
- For a molecule in the first excited state, both the radiative and non-radiative decays to the ground state are possible. Transition  $1 \xrightarrow{nr} 0$  occurs if  $r \leq P_{10nr}$ , and if  $P_{10nr} < r \leq (P_{10nr} + P_{10r})$ , The radiative transition of  $1 \xrightarrow{r} 0$  takes place.

Once a transition occurs, the occupation numbers  $n_0, n_1$ , and  $n_2$  are correspondingly reset, e.g.,  $0 \xrightarrow{\text{absorb}} 2$  is associated with resetting numbers as  $n_0 = 0$  and  $n_2 = 1$ . At the onset of transitions  $2 \xrightarrow{\text{absorb}} 0$  and  $1 \xrightarrow{\text{absorb}} 0$ ,  $\mathbf{p}$  and the first time derivative of  $\mathbf{p}$  are also set to zero. In addition, wave packets with the central frequency equal to emission frequency of the fluorophore  $\omega_e$  are emitted from point sources at the position

of the molecules for which the radiative transition occurs. During emission, the re-excitation of the corresponding molecule is prevented by setting its emission flag to 1 and the state of the molecule is not checked. Emission continues until the emitted wave packet vanishes. At this moment, the emission flag is off and the molecule is at its ground state. The flowchart illustrated in Fig. 2, presents the implemented algorithm in more details.

In this work, an FDTD package has been developed using C++ language. Convolutional perfectly matched layer (CPML) [43,44] boundary condition is used for reducing the reflection from exterior boundaries of the simulation domain while the total-field/scattered-field technique and the Drude-Lorentz model are implemented to handle the incident field and dispersive materials, respectively [40]. Here, the number of fluorophores associated with each grid cell is proportional to the density of the fluorescent material at the same point within the FDTD discretized domain. Therefore, it will be possible to have various fluorescent densities at different locations of the structure.

## 2.1. Validation

For the sake of validation, the present method is applied to a photonic crystal (PC) constructed by triangular arrangement of polystyrene spheres of 500 nm diameter, which is placed on a 200 nm thick silver slab to form an HPPS (Fig.3). The capability of this structure in producing a coherent light from fluorescent spontaneous emissions was previously reported by Shi et al. [28]. To the best of authors' knowledge, this is one of the most prominent publication addressing the coherence of fluorescence emission. In this case, the fluorescent material, fluorophore-doped polyvinil alcohol (PVA), forms a 50 nm thick layer on top of the HPPS and also fills the vacancy between spheres. In order to keep the numerical test-case substantially similar to the reported experimental setup, all parameters of the fluorophores, e.g. decay time constants, emission frequency, and excitation frequency, are set according to the physical attributes of Sulforhodamine 101 (S101).

In order to estimate the degree of temporal coherence, two different approaches has been employed; in one approach, the temporal coherence function (TCF) is utilized, which is the auto correlation of the signal,

$$\Gamma(\tau) = \langle u(t + \tau)u^*(t) \rangle,$$

where angle brackets and superscript \* denote the time averaging and complex conjugate, respectively [45]. Here,  $u(t)$  is the electric field. The degree of coherence is conclusively determined as  $\gamma(\tau) = \Gamma(\tau)/\Gamma(0)$  and thus, the coherence time is

$$\tau_c = \int_{-\infty}^{\infty} |\gamma(\tau)|^2 d\tau. \quad (7)$$

Using this approach for the present test-case, the coherence time is  $\tau_c = 1.14 \times 10^{-13}$  sec, this is approximately equivalent to the wavelength bandwidth of  $|\Delta\lambda| = 6.9$  nm. In the other approach, the desirable wavelength spectrum is

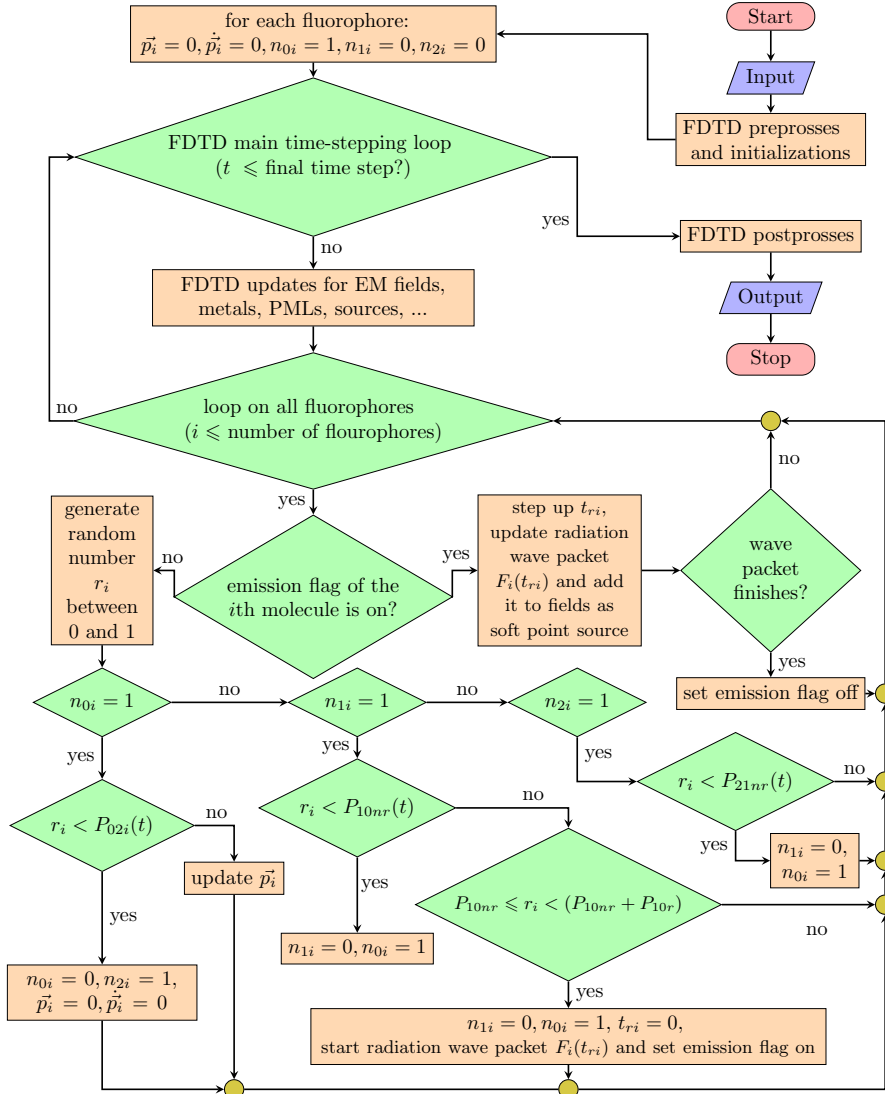


**Figure 2** The algorithm proposed for the implementation of the fluorescence effect within the framework of the developed FDTD method. In each time step, if the emission flag of a fluorophore (e.g. the  $i$ th one) is on, the emission continues. If the flag is off, the state of the molecule should be checked. In case the molecule is at its ground state, the absorption probability  $P_{02i}(t)$  is compared to a randomly generated number,  $r_i$ , and consequently, either the transition to level 2 takes place or the dipole moment of the fluorophore is updated. In other cases (i.e. the molecule is in level 1 or 2) the same procedure is followed with the respective probability functions.

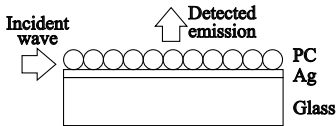


**Figure 3** Schematic of the structure that is used for validation test-case of the proposed numerical method, which was previously experimentally studied by Shi et al. [28].

obtained using the Fourier transform of the time-varying electric field. For the present test-case, this spectrum is shown in Fig.4. By fitting a Gaussian function into the fig-

ure, the emission bandwidth of the peak is calculated to be approximately  $|\Delta\lambda| = 7.1$  nm.

It must be noted that in the present work, a perfectly ordered structure is modeled while any experimental test is subject to fabrication defects. These structural defects lead to a wider bandwidth and therefore, a lower temporal coherence can be detected for the experimental setup. This is due to the fact that any defect/disorder perturbs the Hamiltonian of the structure, which in turn broadens the band of energy [46]. Considering this issue, there is a good agreement between the result obtained using the proposed numerical method and that reported in the literature [28].

On the other hand, the most reliable and extremely practical approach to the estimation of spatial coherence is the Young double slits technique [47] for which, the interfer-

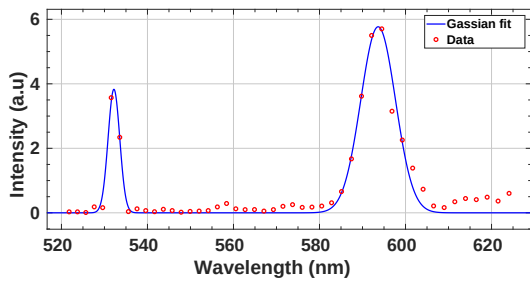


**Figure 4** Wavelength spectrum of reflection obtained using the proposed numerical method for the structure previously studied by Shi et al. [28]. The pick corresponds to the unabsorbed portion of the excitation wave is observed at  $\lambda = 532$  nm and the emission pick occurs at  $\lambda = 594$  nm.

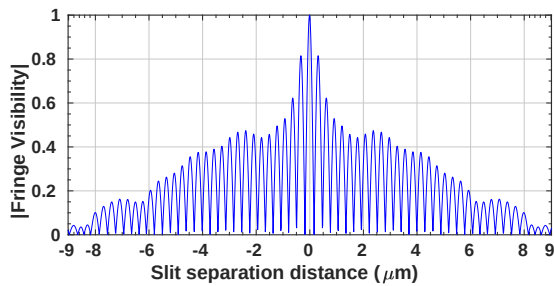


**Figure 5** Young double-slits fringe visibility as a function of the separation distance of the double-slits calculated using the proposed numerical method for the structure previously studied by Shi et al. [28]

ence fringe visibility is analytically calculated as a function of the separation distance between slits as [45]

$$\mathcal{V}_{ij} = \frac{2\sqrt{u_i^2(t)u_j^2(t)}}{u_i^2(t) + u_j^2(t)} M_{ij}.$$

In this equation,

$$M_{ij} = \frac{\langle u_i(t)u_j^*(t) \rangle}{\sqrt{\langle u_i^2(t) \rangle \langle u_j^2(t) \rangle}}$$

is the mutual coherence function between electric fields  $u_i(t)$  and  $u_j(t)$  detected at two distinct points  $i$  and  $j$  placed on a plane perpendicular to the direction of detection, which represent the positions of the slits. For the present test-case, the fringe visibility is plotted in Fig. 5. It is evident that visibility significantly decreases as the slits separation distance increases beyond  $4 \mu\text{m}$  and practically, no interference pattern can be observed for a separation distance of larger than  $8 \mu\text{m}$ . This is in close agreement with the result reported in the reference [28]. Nevertheless, it is noteworthy that using numerical simulation, it can be observed (Fig.5) how the fringe visibility varies for a wide range of separation distances.

The above statements apparently confirm the validity of results obtained by the proposed numerical method and

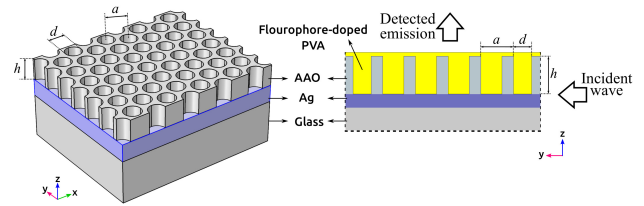


**Figure 6** The overall 3D view of the proposed hybrid anodic structure (left) and its  $yz$  cross-section (right).

clearly shows its excellent performance on simulating the interaction between EM field and fluorescence. Anyhow, this numerical method facilitates studying the statistical characteristics of an ensemble of fluorophores, which is essential for advancements in the field of fluorescence coherence.

### 3. Hybrid Anodic Aluminum Oxide Structure

Here, the proposed method is applied to a novel HPPS that is constructed by placing an inverse photonic crystal, made by pore-opened [48] anodic aluminum oxide (AAO), on top of a 200 nm thick silver (Ag) layer (Fig.6). The cylindrical holes of PC are filled with S101-doped PVA, which also forms a layer of 50 nm thickness on top of the AAO. The structural parameters, i.e., thickness of AAO layer  $h = 500$  nm, diameter of cylindrical holes  $d = 200$  nm, and the center-to-center distance the neighboring cylinders  $a = 250$  nm, have been set in a way that not only the structure can be easily fabricated, but also, it significantly enhances the coherence as seen in the rest of this paper.

Similar to the previous test-case, the proposed HPPS experiences an incident continuous EM wave with a wavelength of 575 nm from its side that is perpendicular to the  $y$ -axis (Fig. 6) and the resulting vertical emission (along  $z$ -axis) is recorded. In this way, the detected wave would not be masked by the incident wave. Moreover, this is a wise choice of the excitation and detection, which is appropriate for imaging and LED applications. In Fig. 7, the recorded field is shown in frequency domain. The graph hits its peak at  $\lambda = 616$  nm with a bandwidth of  $|\Delta\lambda| = 3$  nm. On the other hand, using TCF (equation 7), a coherence time of  $\tau_c = 2.1 \times 10^{-13}$  sec or equivalently  $|\Delta\lambda| = 4$  nm is calculated. It is observed that the presence of the proposed HPPS leads to an almost eight times greater coherence length for the fluorescence emission.

In order to identify the underlying cause of the emergence of such a narrow emission bandwidth, all modes propagated horizontally (along the  $xz$  plane) in PC of the proposed HPPS are also calculated and shown in Fig. 8. It is known that there is no possibility for p-polarized modes to be vertically propagated since the associated electric field is aligned with  $z$ -axis. On the other hand the electrical field is directed horizontally for s-polarized modes and thus, for each wavelength that the horizontal propagation is prevented by HPPS, a vertical reflection is possible. Therefore, considering that the excitation input wave is aligned with  $y$ -axis,

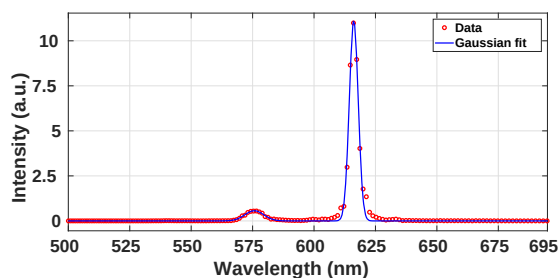


**Figure 7** Wavelength spectrum of the detected wave obtained for the proposed HPPS. The emission pick is observed at  $\lambda = 616$  nm, while a lower pick occurs at  $\lambda = 575$  nm that corresponds to the unabsorbed portion of the excitation wave.

one should focus on the y-directed s-polarized propagation graph in Fig. 8, which reveals a trough at  $\lambda = 616$  nm. In this sense, the portion of the emission band of S101 molecules that coincides with this trough is expected to reflect vertically while the rest propagates along the metal surface. Since for S101 molecules, the excitation band overlaps partially with the emission band, the horizontally propagated modes can excite the neighboring fluorophores. This synchronizes the transitions of the molecules and therefore, a spatial coherence is also expected. The visibilities obtained as results of the double-slits tests are shown in Fig. 9, which clearly shows a spatial coherence width of greater than  $10 \mu\text{m}$ . Anyway, this coherence width is proportional to the propagation length of the horizontally propagated modes, which is determined by the imaginary part of the corresponding wave-vectors. It can state that in the near-field, the plasmonic modes are responsible for coherence while the s-polarized modes are capable to transfer this coherence to the far-field. It must also be noted that the conversion between the s- and p-polarized modes is possible due to the random orientation of the dipole moment of the molecules and internal reflections inside cavities. It is worth noting that the wider the spectral range of the horizontally propagated modes, the larger the portion of energy absorbed by structure. This is the case for the proposed HPPS as seen in Fig. 8, where only a small portion of modes (corresponding to the troughs) is prevented from being horizontally propagated, and thus, a large portion of the incident energy is responsible for exciting the fluorophores (see Fig. 7). This is also among desirable features of the proposed HPPS compared to the previously proposed structures.

As mentioned earlier, one of the most important features of the proposed structure is associated with its adaptable geometry, which can be adjusted in a way that fluorescence coherence is achieved for a different spontaneous emitter; by slightly changing the diameter and center-to-center distance of the cavities, the peaks and troughs of the reflection graphs are shifted. Once the emission frequency coincides with a new trough, coherence is achieved for the emitter of interest based on the above discussions.

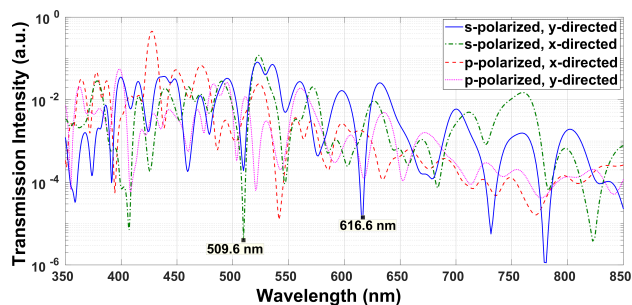


**Figure 8** Wavelength spectrum of horizontally propagated modes in PC of the proposed HPPS obtained for different directions of propagation in  $xy$ -plane with either s- or p-polarizations.

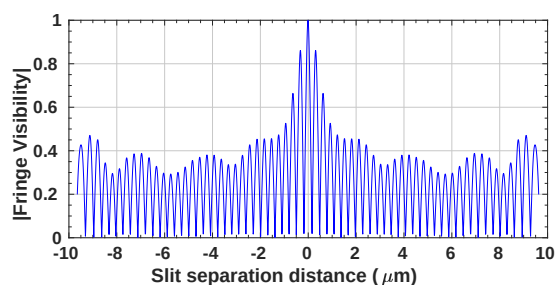


**Figure 9** Young double-slits fringe visibility as a function of the separation distance of the double-slits obtained for the proposed HPPS.

## 4. Conclusion

In this paper, the idea of obtaining coherent light from fluorescence emission using an HPPS is extended by utilizing the AAO structure as the photonic-crystal part of the HPPS. Comparing to the colloidal structure, the proposed HPPS benefits from a more robust structure and can more easily be fabricated with a lower cost, while resulted in significantly enhanced temporal and spatial coherence. The cylindrical cavities lead to a narrow emission spectrum (approximately 4 nm) and therefore, the temporal coherence is improved. Moreover, the synchronized emission of the molecules, which is caused by plasmonic modes and directed along the vertically aligned cavities leads to an enhanced spatial coherence (with the width of larger than  $10 \mu\text{m}$ ).

The present study became possible using the proposed numerical algorithm implemented within the framework of the finite-difference time-domain method that can successfully handle the probabilistic nature of molecular transitions. An interesting but still open topic is the phase transition from incoherence to coherence, which necessarily requires to study a wide range of parameters. Numerical simulation can provide an efficient means for such a study by considerably alleviating the costs associated with experiments. Anyhow, to the best of authors' knowledge, the proposed numerical algorithm is the only one capable of handling this class of simulations.

## References

- [1] V. I. Shcheslavskiy, M. V. Shirmanova, V. V. Dudenkova, K. A. Lukyanov, A. I. Gavrina, A. V. Shumilova, E. Zayaynova, and W. Becker, *Opt. Lett.* **43**(13), 3152–3155 (2018).
- [2] D. A. Giljohann and C. A. Mirkin, *Nature* **462**(7272), 461–464 (2009).
- [3] T. Ribeiro, C. Baleizão, and J. P. S. Farinha, *Scientific Reports* **7** (2017).
- [4] R. J. Moerland, L. Eguiluz, and M. Kaivola, *Optics express* **21**(4), 4578–4590 (2013).
- [5] T. Zhao, K. Yu, L. Li, T. Zhang, Z. Guan, N. Gao, P. Yuan, S. Li, S. Q. Yao, Q. H. Xu et al., *ACS applied materials & interfaces* **6**(4), 2700–2708 (2014).
- [6] L. Wang, Q. Song, Q. Liu, D. He, and J. Ouyang, *Advanced Functional Materials* **25**(45), 7017–7027 (2015).
- [7] M. Bauch, K. Toma, M. Toma, Q. Zhang, and J. Dostalek, *Plasmonics* **9**(4), 781–799 (2014).
- [8] M. K. Kwon, J. Y. Kim, B. H. Kim, I. K. Park, C. Y. Cho, C. C. Byeon, and S. J. Park, *Advanced Materials* **20**(7), 1253–1257 (2008).
- [9] A. Kinkhabwala, Z. Yu, S. Fan, Y. Avlasevich, K. Müllen, and W. Moerner, *Nature Photonics* **3**(11), 654–657 (2009).
- [10] H. Aouani, O. Mahboub, E. Devaux, H. Rigneault, T. W. Ebbesen, and J. Wenger, *Nano letters* **11**(6), 2400–2406 (2011).
- [11] G. Lozano, D. J. Louwers, S. R. Rodríguez, S. Murai, O. T. Jansen, M. A. Verschuuren, and J. G. Rivas, *Light: Science & Applications* **2**(5), e66 (2013).
- [12] L. Langguth, D. Punj, J. Wenger, and A. F. Koenderink, *ACS nano* **7**(10), 8840–8848 (2013).
- [13] P. Anger, P. Bharadwaj, and L. Novotny, *Physical review letters* **96**(11), 113002 (2006).
- [14] T. Pons, I. L. Medintz, K. E. Sapsford, S. Higashiya, A. F. Grimes, D. S. English, and H. Mattoussi, *Nano letters* **7**(10), 3157–3164 (2007).
- [15] X. Li, J. Qian, L. Jiang, and S. He, *Applied Physics Letters* **94**(6), 063111 (2009).
- [16] P. Reineck, D. Gómez, S. H. Ng, M. Karg, T. Bell, P. Mulvaney, and U. Bach, *ACS nano* **7**(8), 6636–6648 (2013).
- [17] S. G. Romanov, A. V. Korovin, A. Regensburger, and U. Peschel, *Advanced Materials* **23**(22-23), 2515–2533 (2011).
- [18] X. Yang, A. Ishikawa, X. Yin, and X. Zhang, *Acs Nano* **5**(4), 2831–2838 (2011).
- [19] Z. Zhang, L. Zhang, M. N. Hedhili, H. Zhang, and P. Wang, *Nano letters* **13**(1), 14–20 (2012).
- [20] A. H. Schokker, F. van Riggelen, Y. Hadad, A. Alù, and A. F. Koenderink, *Physical Review B* **95**(8), 085409 (2017).
- [21] X. Zhu, F. Xie, L. Shi, X. Liu, N. A. Mortensen, S. Xiao, J. Zi, and W. Choy, *Optics letters* **37**(11), 2037–2039 (2012).
- [22] M. López-García, J. F. Galisteo-López, A. Blanco, J. Sánchez-Marcos, C. López, and A. García-Martín, *small* **6**(16), 1757–1761 (2010).
- [23] B. Ding, C. Hrelescu, N. Arnold, G. Isic, and T. A. Klar, *Nano letters* **13**(2), 378–386 (2013).
- [24] S. B. Raghunathan, H. F. Schouten, and T. D. Visser, *Optics letters* **37**(20), 4179–4181 (2012).
- [25] J. J. Greffet, R. Carminati, K. Joulain, J. P. Mulet, S. Mainy, and Y. Chen, *Nature* **416**(6876), 61–64 (2002).
- [26] M. De Zoysa, T. Asano, K. Mochizuki, A. Oskooi, T. Inoue, and S. Noda, *Nature Photonics* **6**(8), 535–539 (2012).
- [27] L. Shi, T. Hakala, H. Rekola, J. P. Martikainen, R. Moerland, and P. Törmä, *Physical review letters* **112**(15), 153002 (2014).
- [28] L. Shi, X. Yuan, Y. Zhang, T. Hakala, S. Yin, D. Han, X. Zhu, B. Zhang, X. Liu, P. Törmä et al., *Laser & photonics reviews* **8**(5), 717–725 (2014).
- [29] L. Shi, X. Liu, H. Yin, and J. Zi, *Physics Letters A* **374**(8), 1059–1062 (2010).
- [30] X. Li, Y. He, T. Zhang, and L. Que, *Optics express* **20**(19), 21272–21277 (2012).
- [31] M. Bradford and J. T. Shen, *Opt. Lett.* **39**(19), 5558–5561 (2014).
- [32] S. Y. Lee and M. A. Mycek, *Opt. Lett.* **43**(16), 3846–3849 (2018).
- [33] J. Lee and J. M. Kosterlitz, *Phys. Rev. Lett.* **65**(Jul), 137–140 (1990).
- [34] T. Schwartz, G. Bartal, S. Fishman, and M. Segev, *Nature* **446**(7131), 52 (2007).
- [35] S. J. Tan, M. J. Campolongo, D. Luo, and W. Cheng, *Nature nanotechnology* **6**(5), 268 (2011).
- [36] M. Sani and M. H. Farzad, *Physical Review B* **97**(8), 085406 (2018).
- [37] P. Genevet, J. P. Tetienne, E. Gatzogiannis, R. Blanchard, M. A. Kats, M. O. Scully, and F. Capasso, *Nano Letters* **10**(12), 4880–4883 (2010).
- [38] D. Wang, T. Yang, and K. B. Crozier, *Optics express* **19**(3), 2148–2157 (2011).
- [39] M. Bauch and J. Dostalek, *Optics express* **21**(17), 20470–20483 (2013).
- [40] A. Taflove and S. C. Hagness, *Computational electrodynamics: the finite-difference time-domain method* (Artech house, 2005).
- [41] A. Jablonski, *Nature* **131**(839-840), 21 (1933).
- [42] J. R. Albani, *Principles and applications of fluorescence spectroscopy* (John Wiley & Sons, 2008).
- [43] J. A. Roden and S. D. Gedney, *Microwave and optical technology letters* **27**(5), 334–338 (2000).
- [44] J. P. Béranger, *IEEE Microwave and Wireless Components Letters* **12**(6), 218–220 (2002).
- [45] J. W. Goodman, *Statistical optics* (John Wiley & Sons, 2015).
- [46] I. Mukherjee and R. Gordon, *Opt. Express* **20**(15), 16992–17000 (2012).
- [47] W. Martienssen and E. Spiller, *American Journal of Physics* **32**(12), 919–926 (1964).
- [48] L. Bruschi, G. Mistura, P. T. M. Nguyen, D. D. Do, D. Nicholson, S. J. Park, and W. Lee, *Nanoscale* **7**, 2587–2596 (2015).